We are IntechOpen,
the world's leading publisher of
Open Access books
Built by scientists, for scientists

6,900
Open access books available

186,000
International authors and editors

200M
Downloads

Our authors are among the

154
Countries delivered to

TOP 1%
most cited scientists

12.2%
Contributors from top 500 universities

Selection of our books indexed in the Book Citation Index
in Web of Science™ Core Collection (BKCI)

Interested in publishing with us?
Contact book.department@intechopen.com

Numbers displayed above are based on latest data collected.
For more information visit www.intechopen.com

Superparamagnetic Behaviour and Induced Ferrimagnetism of LaFeO₃ Nanoparticles Prepared by a Hot-Soap Technique

Tatsuo Fujii, Ikko Matsusue and Jun Takada

Additional information is available at the end of the chapter

1. Introduction

Lanthanum orthoferrite, $LaFeO_3$, is one of the most common perovskite-type oxides having an orthorhombic perovskite structure (space group Pbnm), where the distortion from the ideal cubic structure occurs to form the tilting of the FeO_6 octahedra. $LaFeO_3$ has much practical interest for electroceramic applications due to their attractive mixed conductivity displaying ionic and electronic defects [1, 2]. The mixed ionic-electronic conductivity of $LaFeO_3$ exhibits a linear response to oxygen pressure and provides oxygen sensor applications [3]. The excellent sensitivity and selectivity towards various toxic gases such as CO and NO_x are observed as well [4]. Moreover, $LaFeO_3$ nanoparticles exhibited good photocatalytic properties such as water decomposition and dye degradation under visible light irradiation [5, 6]. These properties are enhanced by the homogeneity and high surface area of the fabricated $LaFeO_3$ particles. Fine particles with diameter of less than 100 nm are potentially required for these purposes.

Besides, the orthoferrites are known to be prototype materials for magnetic bubble devices because of their large magnetic anisotropy with small magnetization [7]. $LaFeO_3$ is an interesting model system of orthoferrite antiferromagnets showing a weak ferromagnetism. The Néel temperature, T_N, of $LaFeO_3$ is 738 K, which is the highest temperature in the orthoferrite family [8]. The magnetic moments of Fe^{3+} ions are aligned antiferromagnetically along the orthorhombic a-axis. But they are slightly canted with respect to one another due to the presence of Dzyaloshinskii-Moriya interaction. A weak ferromagnetic component parallel to the c-axis appears. The magnetization of $LaFeO_3$ bulk crystals is considerably small, 0.044 μ_B/Fe [8]. However, magnetic structures of small particles are often different

from those of bulk ones. For instance, antiferromagnetic nanoparticles exhibit increasing net magnetization due to the presence of uncompensated surface spins [9, 10]. If the ferromagnetic behavior is promoted in $LaFeO_3$, it should provide facile handling of their applications by using magnetic field. Magnetic properties of well-defined $LaFeO_3$ nanoparticles are worthy to investigate.

It is well known that the wet-chemical methods offer large advantages for low-temperature oxide formation with high surface area, small particle size, and exact cation-stoichiometry. Several methods such as co-precipitation technique [11, 12], polymerized complex method [13], combustion synthesis [14], and sol-gel technique [15] were reported to prepare $LaFeO_3$ nanoparticles. For instance the formation of a single phase of $LaFeO_3$ with the perovskite structure was observed at lower calcination temperatures of 300°C in [11, 12]. This temperature was much lower than that of conventional solid state reaction method. Recently we have successfully prepared $LaFeO_3$ nanoparticles by using the new chemical synthesis method, so-called "hot soap method" [16, 17]. It showed high controllability over the formation of nanoparticles with narrow size distribution, which was performed in the presence of surfactant molecules at high temperatures. The hot soap method is based on the thermal decomposition of reaction precursors of organometallic compounds in polyol solvent. But the presence of surfactant molecules in the solution prevents aggregation of precursors during growth. It was widely applied to prepare nanoparticles of compound semiconductors [18] and metallic alloys [19]. However there were few reports on preparing oxide nanoparticles [20].

In this paper we describe the details of our synthesis procedure of $LaFeO_3$ nanoparticles by using the hot soap method. The magnetic properties of the resultant particles were also discussed as a function of the particle sizes.

2. Experiment

$LaFeO_3$ nanoparticles were synthesized by the hot soap method. Their synthesis procedure is outlined in Figure 1. All chemicals used in this experiment were of reagent grade and used without any further purification. Iron acetylacetonate ($Fe(acac)_3$) and lanthanum acetate ($La(ac)_3 \cdot 1.5H_2O$) were preferred as iron and lanthanum sources, respectively, that were soluble in organic solvents such as polyethylene glycol (PEG 400). In a typical synthesis procedure, equal amounts of $Fe(acac)_3$ (1.2 mmol) and $La(ac)_3$ (1.2 mmol) were weighed out accurately and charged into a reaction flask with 20 mL of PEG 400. Coordinating organic protective agents of oleic acid (5 mmol) and oleylamine (5 mmol) were injected into the reaction mixture and the transparent brown solution was observed. Thereafter, the mixture solution was raised to 200°C and maintained for 3 h with stirring. Before cooling down to room temperature, 50 mL of ethanol was added to the reaction mixture, in order to precipitate the particles. The precipitated particles were rinsed with ethanol and dried at 100°C for 1 h. Some of the sample powders were heat-treated in air for 6 h at various temperatures between 300 and 500°C.

Obtained sample powders were characterized by x-ray powder diffraction (XRD) with monochromatic Cu Kα radiation, infrared spectroscopy (IR), and thermogravimetry and differential thermal analysis (TG-DTA). Powder morphologies of the products were observed by scanning electron microscopy (SEM, Hitachi S-4300) at 20 kV and transmission electron microscopy (TEM, Topcon EM-002B) at 200 kV. The BET surface areas were measured by using N_2 absorption at 77 K. The magnetic properties were investigated using a vibrating sample magnetometer with high-sensitivity SQUID sensor (MPMS SQUID-VSM) and conventional transmission Mössbauer spectroscopy with a 925 MBq ^{57}Co/Rh source. The velocity scale of Mössbauer spectra was calibrated with reference to α-Fe.
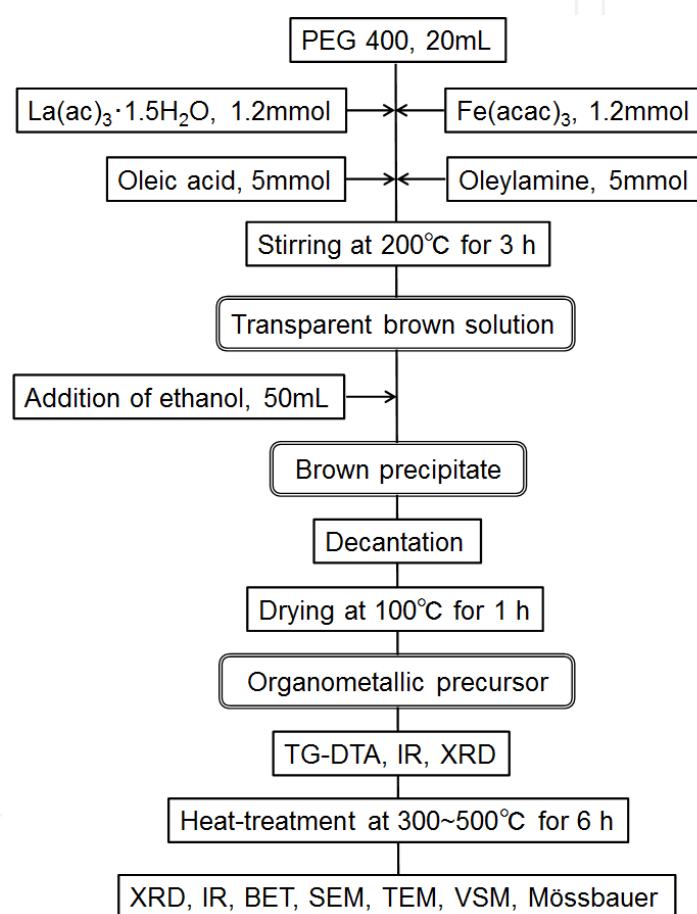
```
                    ┌─────────────────┐
                    │  PEG 400, 20mL  │
                    └─────────────────┘
┌──────────────────────────┐    ┌─────────────────────┐
│ La(ac)₃·1.5H₂O, 1.2mmol  │→  ←│ Fe(acac)₃, 1.2mmol  │
└──────────────────────────┘    └─────────────────────┘
┌──────────────────────────┐    ┌─────────────────────┐
│    Oleic acid, 5mmol     │→  ←│  Oleylamine, 5mmol  │
└──────────────────────────┘    └─────────────────────┘
            ┌──────────────────────────┐
            │  Stirring at 200°C for 3 h │
            └──────────────────────────┘
            ┌──────────────────────────┐
            │ Transparent brown solution │
            └──────────────────────────┘
┌──────────────────────────┐
│ Addition of ethanol, 50mL │→
└──────────────────────────┘
              ┌──────────────────┐
              │ Brown precipitate │
              └──────────────────┘
              ┌──────────────────┐
              │    Decantation   │
              └──────────────────┘
            ┌──────────────────────┐
            │ Drying at 100°C for 1 h │
            └──────────────────────┘
            ┌──────────────────────────┐
            │ Organometallic precursor  │
            └──────────────────────────┘
              ┌──────────────────┐
              │  TG-DTA, IR, XRD  │
              └──────────────────┘
        ┌──────────────────────────────────┐
        │ Heat-treatment at 300~500°C for 6 h │
        └──────────────────────────────────┘
      ┌──────────────────────────────────────────┐
      │ XRD, IR, BET, SEM, TEM, VSM, Mössbauer    │
      └──────────────────────────────────────────┘
```

Figure 1. Flowchart of the procedure to prepare LaFeO₃ nanoparticles.

3. Results and discussion

3.1. Thermal decomposition of organometallic precursor

Figure 2 shows the TG-DTA curves of the organometallic precursor obtained by the hot soap method. In the TG curve, there are four temperature regions based on weight loss: (1) RT ~ 220°C, (2) 220 ~ 420°C, (3) 420 ~ 510°C, and (4) 510 ~ 600°C, in which the corresponding organic weight loss of 4%, 38%, 45% and 1% were observed, respectively. The small weight loss of the region (1) was ascribed to the evaporation of residual water and ethanol. While

the large weight loss of the region (2), accompanied with faint endo- or exothermal peaks in the DTA curve, corresponded to the sublimation and the decomposition of excessive organic substances such as PEG, oleic acid and oleylamine. The temperature range of the region (2) was coincident with the boiling points of individual substances of 250°C (PEG), 223°C (oleic acid) and 350°C (oleylamine). The region (3) comprised the combustion reaction of the residual organics and carbonate components as suggested by the large exothermal peaks at 460°C and 500°C. The large weight loss was due to the decomposition of the most of the organics by oxidation and the release of NO_x, H_2O, CO and CO_2 gases, together with the formation of $LaFeO_3$ as discussed latter. Further heat-treatment in the region (4) gave no major weight loss anymore.
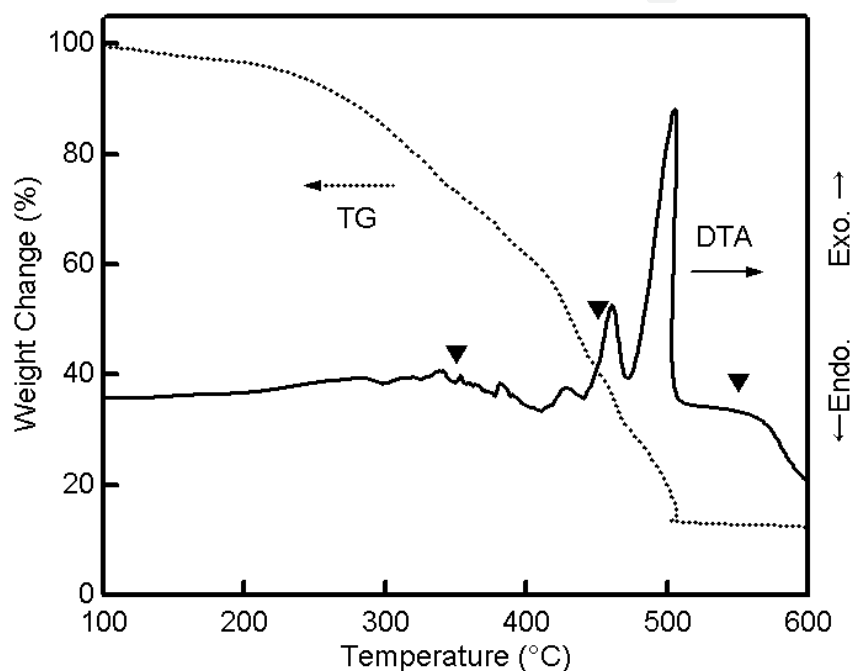
Figure 2. TG-DAT curves of the precursor. The solid triangles indicate the set temperatures for the subsequent XRD and IR observations.

In order to identify the structural changes of the resultant precursor after the heat-treatment, we measured XRD and IR spectra of heat-treated samples taken out from the TG-DTA furnace immediately after reaching to the set temperatures. Figure 3 shows the XRD patterns of the heat-treated samples at various set temperature by TG-DTA. The XRD pattern of the precursor powder had no sharp diffraction lines resulting from the formation of perovskite type oxides. The broad bands centered at around $2\theta = 30°$ and $45°$ suggested the existence of disordered La_2O_3 phase [21]. Scarce changes in XRD patterns were observed up to the heating of 450 °C. However the XRD pattern of the specimen heated at 550 °C showed clear peaks attributed to $LaFeO_3$ perovskite phase. The pattern showed only the presence of the orthorhombic $LaFeO_3$ phase without the broad bands. Observed crystallization temperature between 450 and 550°C was very consistent with the thermal decomposition temperature of the precursor associated with the large exothermal peaks on the corresponding TG-DTA curves (Figure 2).
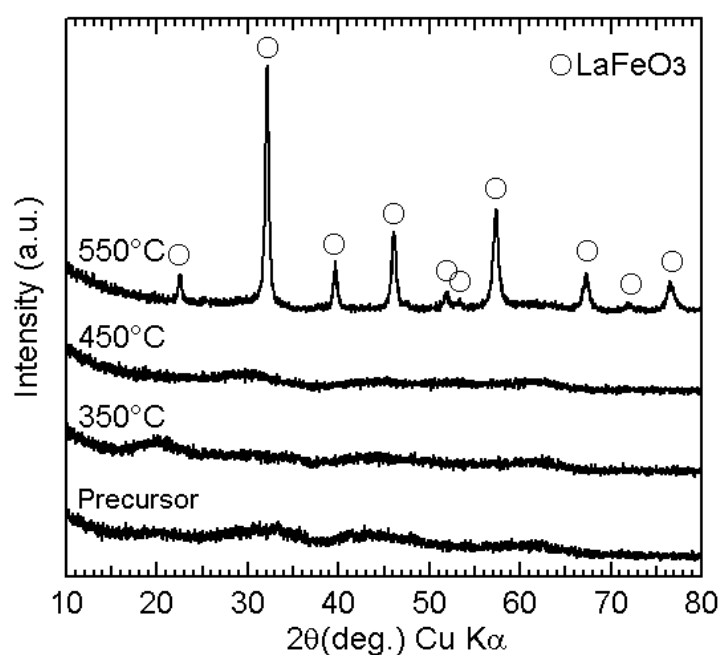
Figure 3. Typical XRD patterns of the obtained products heat-treated at various set temperatures in TG-DTA furnace with no holding time.
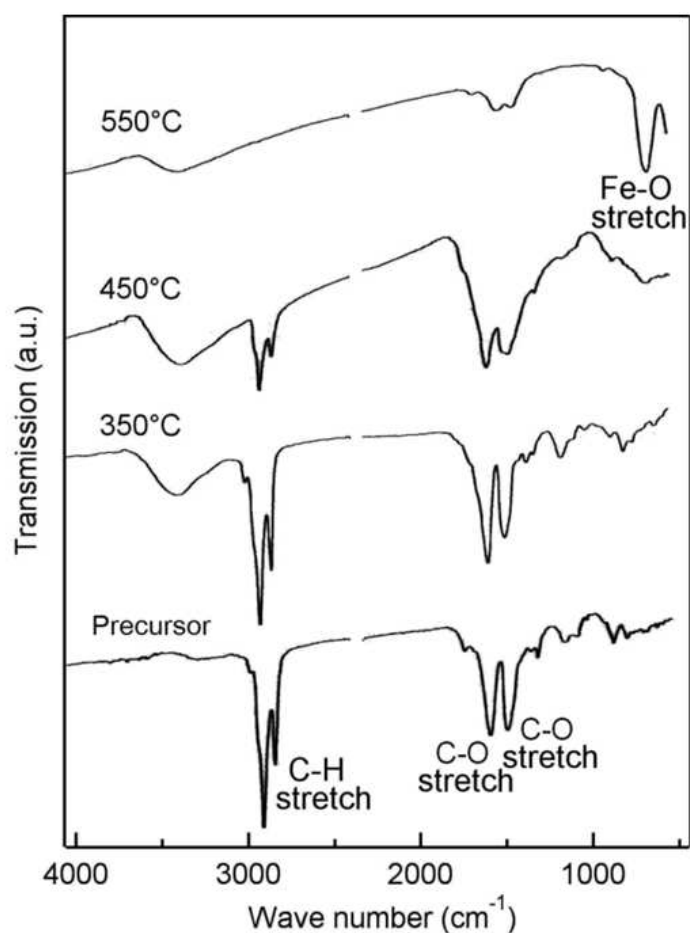

Figure 4. Corresponding IR spectra of the obtained products shown in Figure 3.

The crystallization of LaFeO₃ was fully accompanied with the decomposition of the organic substances. The corresponding IR spectra of the heat-treated samples at various set temperatures of TG-DTA are shown in Figure 4. The IR spectra clearly provided the evidence for the presence of organic substances in the precursor. The strong absorption bands at about 2900 cm^{-1} were assigned to the olefinic C-H stretching bands. While the bands appearing at 1400 ~ 1600 cm^{-1} were characteristics of the metal chelate compounds with carbonyl groups [22, 23]. Two strong peaks at 1550 and 1450 cm^{-1} were mainly assigned to the C=O asymmetric and symmetric stretching modes, respectively. The metal ions in the precipitate could be coordinated with large amount of organic molecules and the large weight loss (87%) at 500°C was confirmed after the thermal decomposition. With increasing the heat-treated temperature, the absorption bands assigned to the organic bonds were gradually decreased in intensity and nearly vanished at 550°C. Besides the strong new band appeared at 600 cm^{-1}, that can be attributed to the Fe-O stretching vibration band due to the formation of LaFeO₃ phase [24]. These results fully agreed with the XRD phase-analysis findings.

3.2. Formation of LaFeO₃ nanoparticles

As shown in Figure 2 in the previous section, a large weight loss of the precipitate started at 220°C, much lower than the temperature of the combustion of the residual organics and the crystallization of LaFeO₃. Moderate decomposition of organic substances in the precursor seemed to start prior to the combustion. The migration of metal ions should be facilitated even at the lower temperature. Therefore the long time heat-treatments below the combustion temperature were conducted to the precursors to prepare nanocrystalline particles. Figure 5 shows the XRD patterns of the samples heat-treated in air for 6 h at various temperatures below the combustion. The sample heated at 325°C showed the diffuse XRD pattern with no crystalline phases. While at 350°C, broad XRD peaks attributed to the LaFeO₃ perovskite phase started to be observed. This temperature was much lower than the crystallization temperature deduced by the TG-DTA curves. The average grain size, t, of LaFeO₃ particles estimated from the XRD peak broadening for the LaFeO₃(121) lines was summarized in Table 1 by using the Scherrer equation: $t = \frac{0.9\lambda}{B\cos\theta}$, where λ is the x-ray wavelength, B is the line broadening at half the maximum intensity (FWHM) in radians, and θ is the Bragg angle. The particle size of LaFeO₃ formed at 350°C was about 16 nm. With increasing the heat-treatment temperature, the XRD peaks became sharper because of the grain growth of the LaFeO₃ particles.

Heat-treatment temperature (°C)	Crystallite size (nm)
350	16
450	20
500	22

Table 1. Average crystallite size of LaFeO₃ nanoparticles as a function of the heat-treatment temperature.
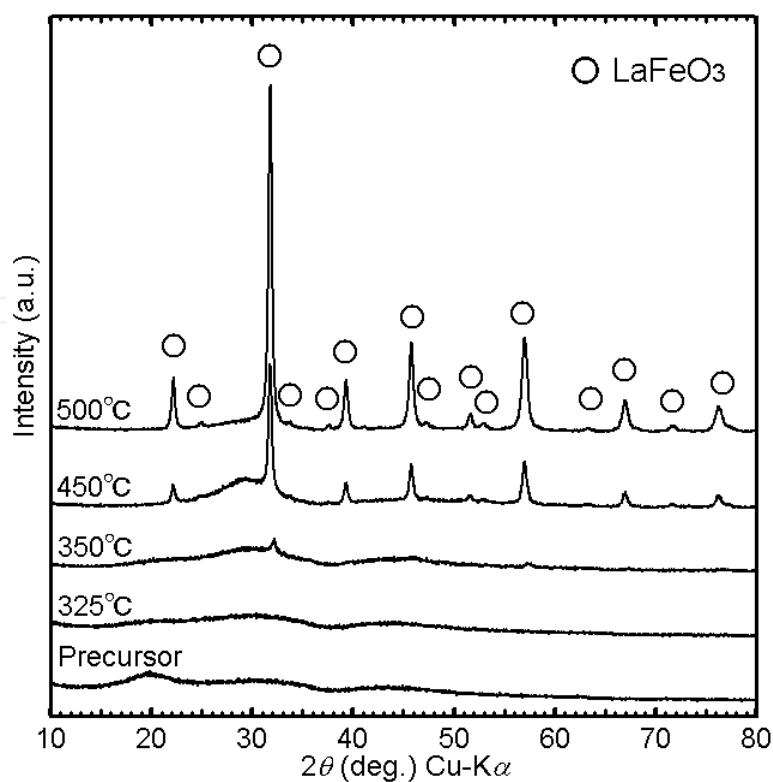
Figure 5. Typical XRD patterns of the obtained products after the long time heat-treatment (6 h) at various temperatures.
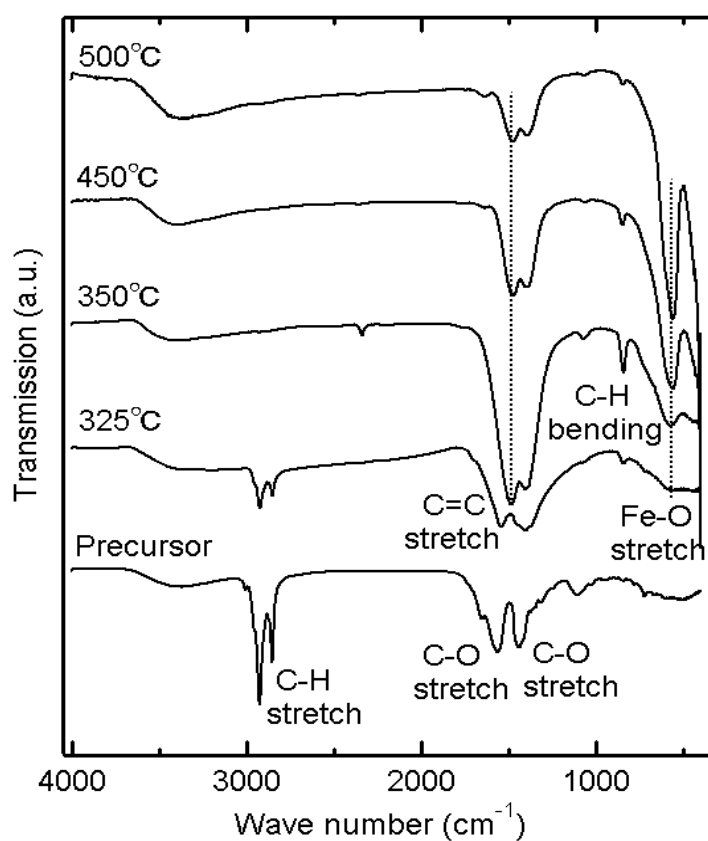

Figure 6. IR spectra of the obtained products after the long time heat-treatment (6 h) shown in Figure 5.

Decomposition of organic substances after the heat-treatment below the combustion temperature was examined by IR spectroscopy. Figure 6 shows the IR spectra of long time (6h) heat-treated samples at various temperatures. The precursor should consist of organometallic composites derived from starting materials. The IR spectrum indicated the clear bands assigned to C-H stretching (~2900 cm^{-1}) and C-O stretching (1400~1600 cm^{-1}) of organic substances [22, 23]. With increasing the heat-treatment temperature, the intensities of initial bands steeply decreased and a new band assigned to Fe-O stretching (~600 cm^{-1}) started to appear at 325°C. This temperature was slightly lower than the formation temperature of $LaFeO_3$ nanoparticles confirmed by XRD observations. And the Fe-O stretching band was intensified monotonically with increasing the temperature. By the way, subsequent to diminishing the intensity of olefinic C-H stretching bands, new strong band appeared in the spectra at 1475 cm^{-1} in addition to a weak band at 843 cm^{-1}. The former band could be assigned to aromatic C=C stretching vibration, while the latter was to aromatic C–H bending one [25]. This result suggested that the framework of organic matrix in precursor was considerably changed after the long time heat-treatment below the combustion temperature. The heat-treatment seemed to promote carbonization of organic substances as well as the crystallization of $LaFeO_3$ nanoparticles.

SEM images of the obtained powders heat-treated in air at various temperatures for 6 h are shown in Figure 7. The precursor particles with and without heat-treatment at 325°C revealed the smooth surface with squamous and wrinkled structures, respectively. These surface morphologies should be very consistent with the amorphous nature of the resultant organic matrix. With increasing the heat-treatment temperature above 350°C, the particles were crowned by squamous surfaces. The macrosized particles seemed to be disaggregated into fine particles after the crystallization. In spite of the nanometric crystal size determined from the XRD profiles, the BET surface area of the obtained $LaFeO_3$ particles at 350 and 500°C were only 3.9 and 3.1 m^2/g, respectively. The nanocrystalline fine particles formed in the precursors were strongly agglomerated with each other in present cases. The residual carbon matrix could also affect the morphology of the obtained powders.

The structure of the $LaFeO_3$ nanocrystallites was further analyzed by TEM micrograph. Figure 8 shows the TEM image and electron diffraction (ED) pattern of $LaFeO_3$ nanoparticles obtained by the long time (6 h) heat-treatment at 350°C. The particulates consisted of an agglomeration of numerous spherical primary particles loosely aggregated together, in contrast to the SEM observations. The average diameter of the primary particles estimated from the TEM image was about 15 nm, which was well consistent with that from XRD. The high-contract dotted rings in the ED patterns indicated the good crystallinity of the $LaFeO_3$ nanoparticles. These rings were indexed as the $LaFeO_3$ perovskite phase with random orientation. No diffraction spots attributed to the secondary phase were observed.

3.3. Magnetic properties of $LaFeO_3$ nanoparticles

Room temperature Mössbauer spectra of obtained powders after the long time heat-treatment (6h) at various temperatures are shown in Figure 9. The sample heated at 500°C, which had a larger crystallite size, showed a clear sextet pattern with a small amount of a
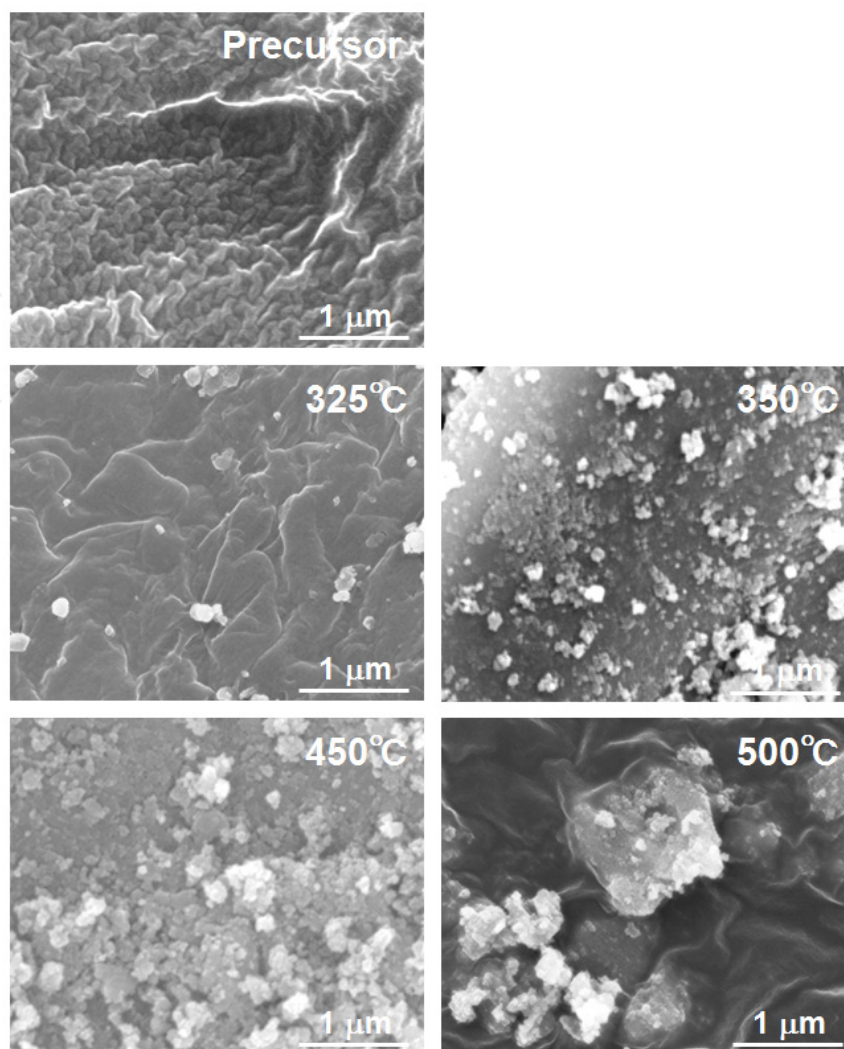
Figure 7. SEM images of the obtained products heat-treated at various temperatures.

doublet component. The observed Mössbauer parameters showing antiferromagnetic ordering were fully consistent with those of the LaFeO₃ bulk crystals [26]. The paramagnetic doublet patterns were dominant for other samples obtained at lower temperatures (350 and 450°C) in spite of the formation of LaFeO₃, as well as the non-crystalline samples at 300 and 325°C. This behavior was attributed to superparamagnetism because of the fine crystallite size of LaFeO₃ as discussed above. By the way, the doublet patterns showed asymmetric profiles. The asymmetric doublets were probably caused by the presence of iron ions in different environments such as surface or inner part of the crystals and/or the non-crystalline matrix. But it was difficult to decompose such complex spectra into unique components. Therefore the spectra were simply analyzed to assume one asymmetric doublet with different widths. The fitted parameters are listed in Table 2. The isomer shift values of ~0.3 mm/s for both doublet and sextet peaks indicated the Fe valence states in the all specimens were trivalent. No reduction occurred during the long time heat-treatment with organic substances. When looking in detail, the Mössbauer parameter of the doublet pattern indicated the systematic change depending on the heat-treatment temperature. The isomer shift gradually decreased while the quadrupole splitting gradually increased with

increasing the heat-treatment temperature. This result suggested the formation of strong Fe-O bonds and ligand fields due to the crystallization of $LaFeO_3$ particles.
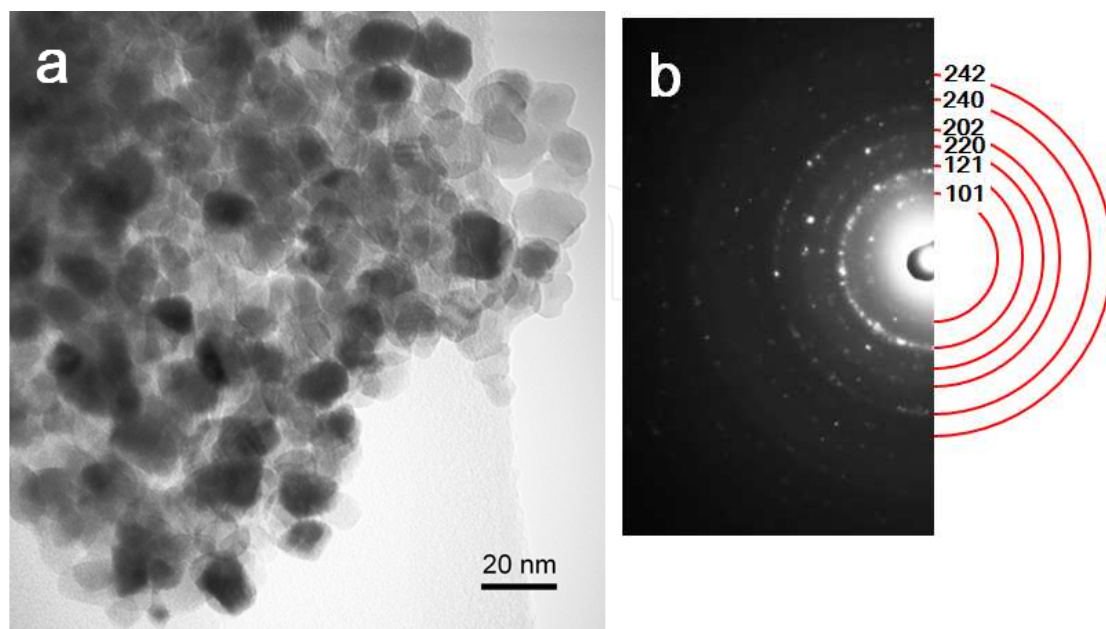

Figure 8. (a) TEM image and (b) its ED pattern of $LaFeO_3$ nanoparticles obtained at 350°C. Diffraction rings are indexed as their corresponding $LaFeO_3$ planes.

Heat-treatment temperature (°C)	Isomer shift (mm/s)	Quadupole splitting (mm/s)	Hyperfine filed (kOe)	Intensity (%)
500	0.369	-	517	65
	0.285	1.051	-	35
450	0.364	-	508	23
	0.292	1.008	-	77
350	0.355	-	512	21
	0.313	0.924	-	79
325	0.329	0.891	-	100
300	0.327	0.824	-	100

Table 2. Fitted Mössbauer parameters obtained from the spectra in Figure 9.

Magnetic measurements were performed on the heat-treated powders at various temperatures. The room-temperature magnetization curves of obtained samples are shown in Figure 10 as a function of the heat-treated temperature. $LaFeO_3$ is known to be antiferromagnetic with weak ferromagnetism [8]. The net magnetization of $LaFeO_3$ should be very small because of the antiferromagnetic order of the Fe^{3+} spins. Only a slight canting of the adjacent Fe^{3+} spins produced weak ferromagnetism. The spontaneous magnetization of $LaFeO_3$ bulk crystals was only ~0.1 emu/g at room temperature [27]. However all samples seemed to have large magnetization, especially for the sample heat-treated at 350°C. The shape of hysteresis loops

showing the small spontaneous magnetization were characteristics of weak ferromagnetism. The maximum field applied of 60 kOe did not saturate the magnetization. This was mainly caused by antiferromagnetic ordering of the spins in the nanoparticles [27]. By the way, the sample prepared at 500°C showed the remarkable hysteresis gap than the other samples. Mössbauer spectra indicated that only the sample prepared at 500°C possessed predominant antiferromagnetic ordering at room temperature while the others were paramagnetic. The small hysteresis gaps of the samples obtained at lower temperatures (325~450°C) supported their superparamagnetic nature.
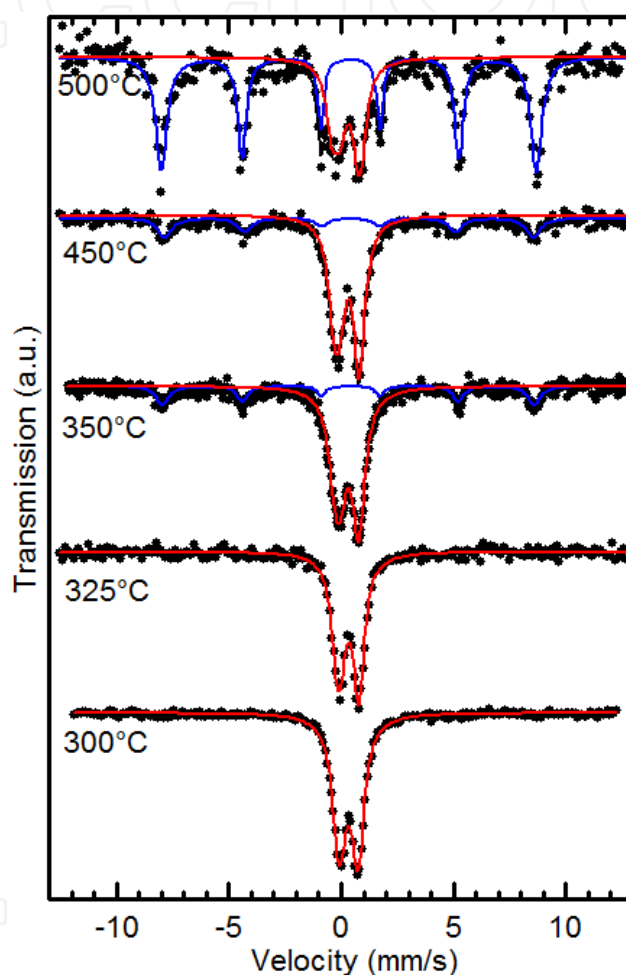
Figure 9. Room temperature Mössbauer spectra of the obtained products heat-treated at various temperatures.

The temperature dependence of magnetization behaviors under zero-field-cooling (ZFC) and field-cooling (FC) conditions measured in an external magnetic field of 200 Oe are shown in Figure 11. Magnetization of LaFeO₃ particles obtained at 500°C was gradually decreased with decreasing the temperature. This behavior was characteristic of the antiferromagnetic ordered states below the T_N. The higher T_N above the room temperature was confirmed by the Mössbauer spectroscopy. The difference of magnetization values between ZFC and FC curves was attributed to the residual paramagnetic components at room temperature. On the other hand, magnetization of other samples obtained at 300~450°C were smoothly increased
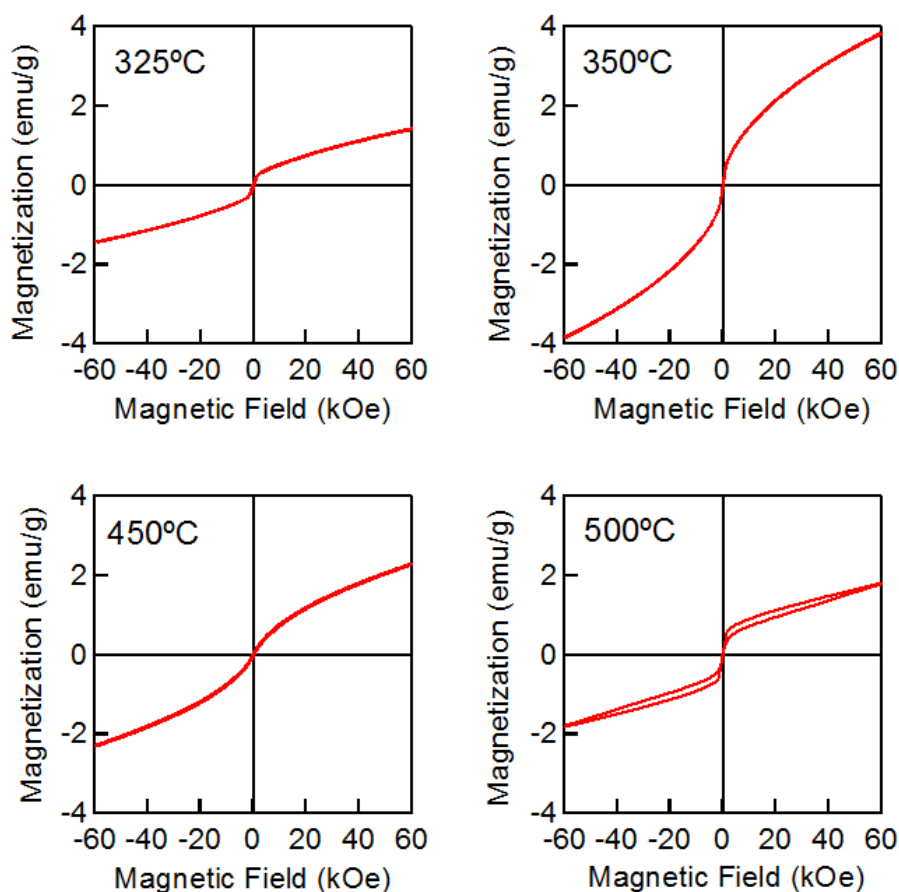
Figure 10. Room temperature magnetization curves of the obtained products heat-treated at various temperatures.

with the decreasing temperature. These behaviors were very consistent with the paramagnetic nature of the obtained samples at room temperature. Moreover, the sharp cusps in the ZFC curves were observed for the samples obtained at 325~450°C. These were considered to be the superparamagnetic blocking temperature (T_B), where the magnetization of $LaFeO_3$ nanoparticles begun to freeze [28]. The T_B detected by the ZFC curves was summarized in Table 3. It was decreased steeply with decreasing the heat-treatment temperature coincident with the decreasing particle sizes. Besides, the observed T_B values were very small, which indicated that the magnetic interactions between the obtained $LaFeO_3$ nanoparticles were very weak. The surface of $LaFeO_3$ nanoparticles was probably coated with the residual organic molecules to form the non-magnetic layers [29]. This assumption was fully supported by the IR spectra indicating the presence of carbonized components and the TEM micrograph showing the loosely aggregating $LaFeO_3$ nanoparticles. It should be mentioned here that the sample heat-treated at 325°C indicated the superparamagnetism, showing the small cusp in the ZFC curve at 7.7 K. The sample seemed to contain the $LaFeO_3$ nanoclusters, though it showed the non-crystalline XRD pattern. But the IR spectrum seemed to have good sensitivity to detect their formation as well as the magnetization measurement. By the way, in the case of conventional superparamagnetic behavior, the FC magnetization curves should increase continuously with decreasing the temperature below the T_B. But the FC curve of the heat-treated sample at 450°C showed a small cusp on cooling as well as the ZFC curve. This

behavior suggested that the antiferromagnetic interactions between nanoparticles were present [28]. Long-range antiferromagnetic order was developed in associate with the grain growth of the LaFeO₃ nanoparticles.

Heat-treatment temperature (°C)	Blocking temperature (K)
325	7.7
350	27.6
450	36.9

Table 3. Blocking temperature (T_B) obtained from the ZFC curves shown in Figure 11.
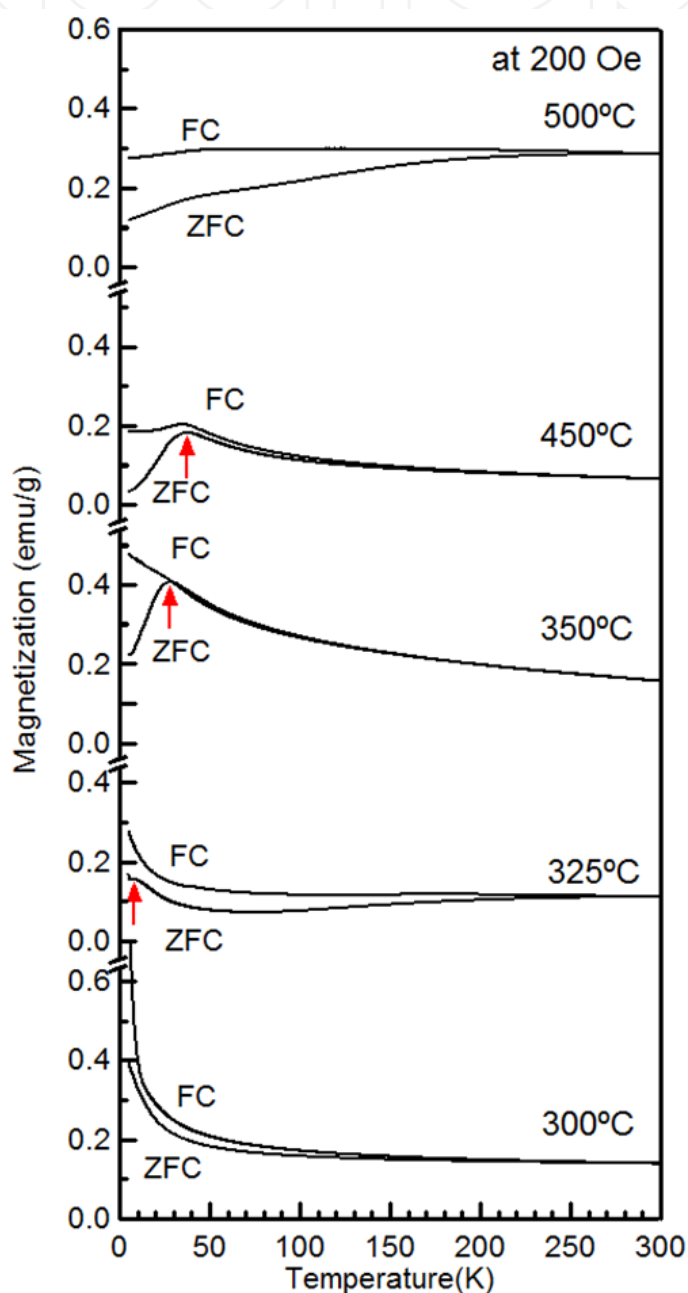
Figure 11. Temperature dependence of ZFC and FC magnetization curves at 200 Oe for the obtained products at various heat-treatment temperatures

In order to demonstrate the superparamagnetic behavior more directly, we measured the temperature dependence of their Mössbauer spectra down to 15 K. Figure 12(a) shows the typical law temperature Mössbauer spectra of the LaFeO₃ nanoparticles obtained at 350°C. The spectrum measured at room temperature (see Figure 9) was well consistent with that of the LaFeO₃ nanoparticles with average grain size of 16 nm reported in literature [26]. The spectrum was mainly composed of the super-paramagnetic doublet peak besides to the magnetically split sextet. The component showing the sharp sextet pattern could be attributed to the unexpected coarse LaFeO₃ particles which had a good crystallinity, while the most of the particles exhibited the paramagnetic doublet pattern at room temperature. With decreasing the temperature, the paramagnetic spectra corresponded to the enlarged sextets due to the presence of magnetic order. Therefore the spectra were decomposed into three components. One was the sharp sextet for the coarse particles; second and third were the broad sextet and paramagnetic doublet for the nanoparticles, respectively. Relative intensity ratio of each component was plotted in Figure 12(b) as a function of the temperature. The relative area of the paramagnetic component varies almost linearly with decreasing the temperature below 100 K. According to the Mössbauer measurements, we defined the
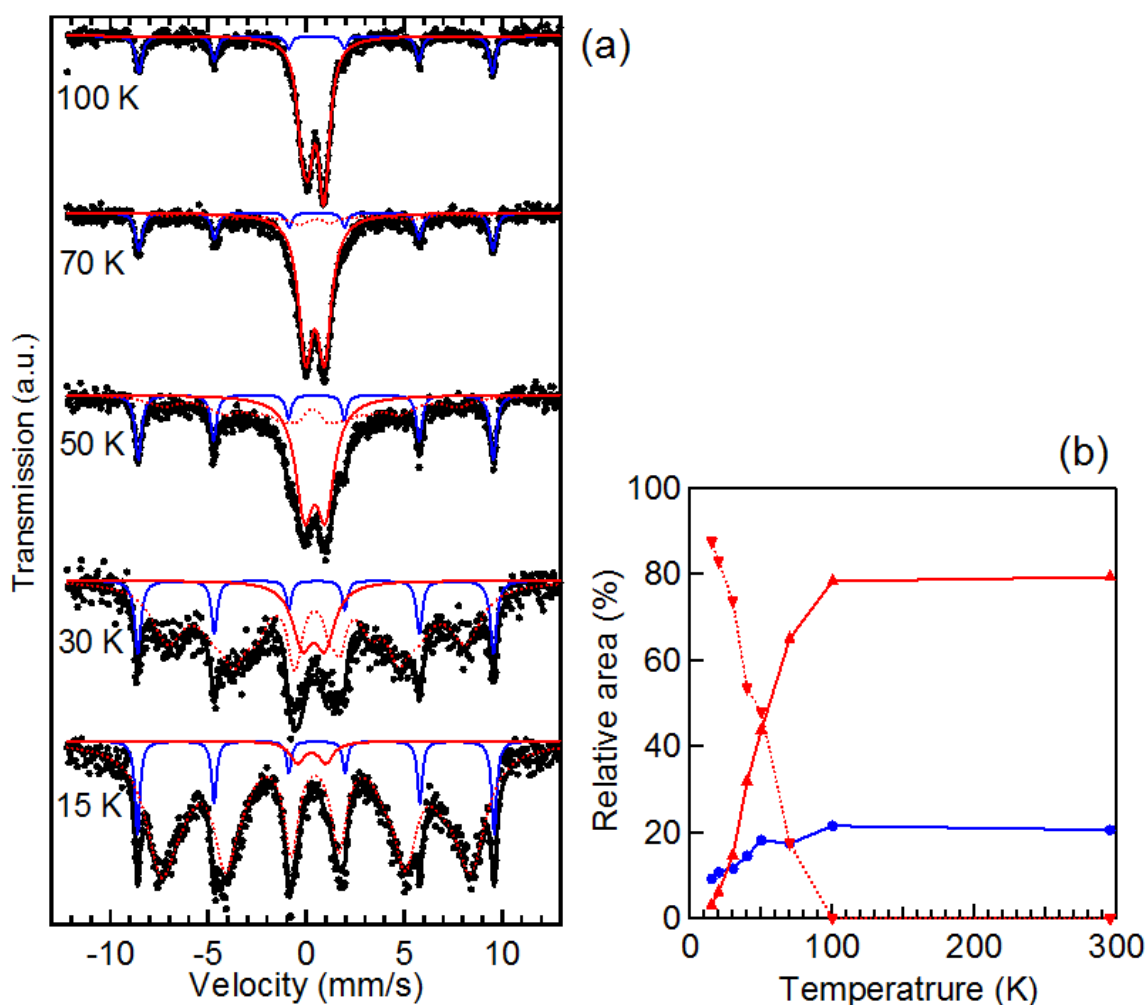

Figure 12. (a) Low temperature Mössbauer spectra of LaFeO₃ nanoparticles obtained at 350°C, and (b) relative area of each component as a function of the temperature. The details are described in the text.

median blocking temperature (T_{Bm}), as a temperature where the doublet collapsed to 50% of its initial value. This analysis yielded the T_{Bm} of ~50 K, which was much higher than the superparamagnetic T_B obtained by the magnetization measurement. It was well-known that the time scale of the superparamagnetic fluctuations becomes comparable to the time scale of the measurement [30]. The time scale of Mössbauer measurements (~10^{-9} s) was much faster than that of magnetization measurements (~10^{-1} s) and gave the higher T_{Bm} well above the T_B. This phenomenon evidenced the presence of superparamagnetic relaxation of the obtained samples.

Figure 13 shows the field dependent magnetization curves measured at lower temperature (5 K) for the LaFeO₃ nanoparticles prepared at various heat-treatment temperatures. The samples showed considerable magnetization at low temperature, though the net magnetization of LaFeO₃ bulk crystals should be very small because of the antiferromagnetic order of the Fe^{3+} spins. A spontaneous magnetization of the bulk crystals was evaluated to 0.15 emu/g at 5 K [16]. We have recently reported that the LaFeO₃ nanoparticles prepared at 350°C revealed an anomalous large spontaneous magnetization of 7.8 emu/g [16]. This phenomenon was almost reproducible. The spontaneous magnetization of the obtained powders exhibited the maximum value for the samples prepared at 350°C. The LaFeO₃ nanoparticles with the average diameter of ~15 nm seemed to have large ferromagnetism instead of antiferromagnetism. The induced ferromagnetism in LaFeO₃ nanoparticles was possibly associated with the uncompensated surface spins as reported in other antiferromagnetic nanocrystalline systems [9, 10]. It should be worth to mention that the induce magnetic moment per Fe^{3+} ion was evaluated to 0.34 μ_B for the sample obtained at 350°C. Taking into account that the moment of Fe^{3+} is 5 μ_B, a large fraction (~7%) of Fe^{3+} ions contribute to the magnetization of LaFeO₃ nanoparticles. Magnetic structure of LaFeO₃ nanoparticles should be strongly modified from the bulk one.

By the way, all magnetization curves revealed clear hysteresis gaps with small loop shifts at 5 K. The coercivity and the exchange bias field of each sample are summarized in Table 4 as well as the spontaneous magnetization. The exchange field was linearly increased with increasing the heat-treatment temperature. The exchange bias was generally attributed to the exchange coupling between the ferromagnetic shell and the antiferromagnetic core of the particles [31]. In the case of LaFeO₃ particles, the uncompensated surface spins and/or the enhanced spin cantings near the surface region should cause the considerable magnetization. With the increasing particle size, the reliable antiferromagnetic core was formed to produce the large exchange coupling.

Heat-treatment temperature (°C)	Spontaneous magnetization (emu/g)	Coercivity (Oe)	Exchange bias (Oe)
325	2.89	823	23
350	5.90	1304	25
450	2.94	2240	64
500	1.40	1275	208

Table 4. Magnetic parameters at 5 K of the obtained products at various heat-treatment temperatures.
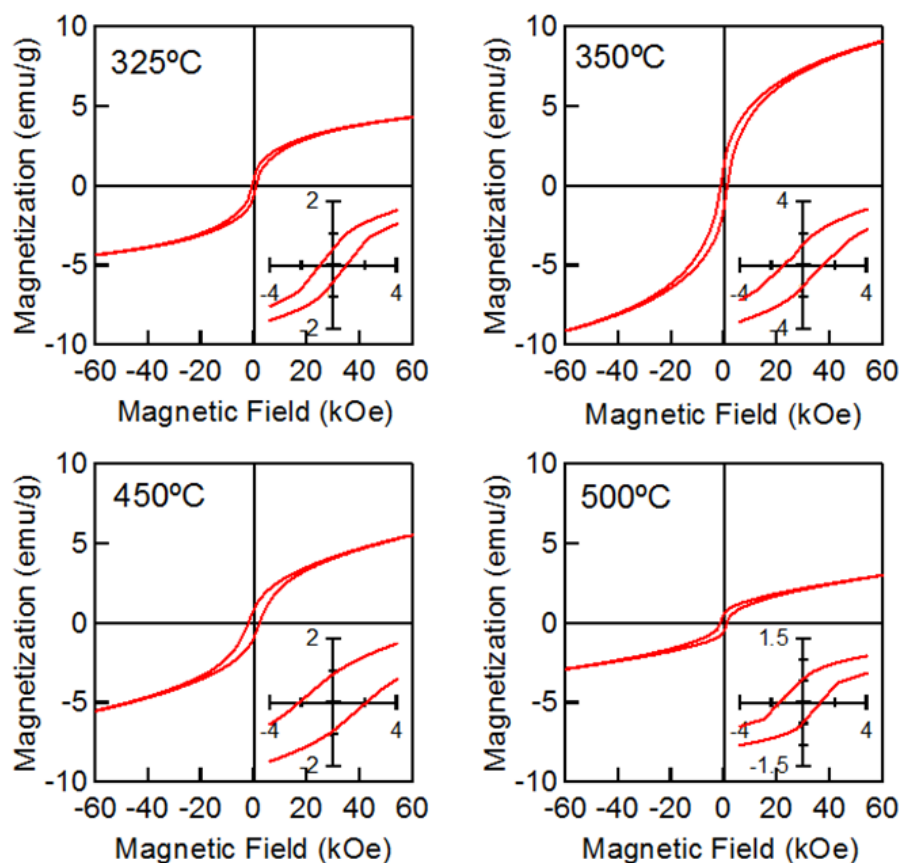
Figure 13. Low temperature (5 K) magnetization curves of the obtained products heat- treated at various temperatures. The insets are the enlarged view of the central region.

4. Conclusion

Nanocrystalline $LaFeO_3$ particles with an average diameter of 16 nm were prepared by using hot-soap technique. Crystalline $LaFeO_3$ were formed at a relatively low heat-treatment temperature of 350°C without any phase segregation. This temperature was much lower than the combustion point of organic substances. With increasing the heat-treatment temperature, the grain size of $LaFeO_3$ particles was increased. The $LaFeO_3$ nanoparticles exhibited superparamagnetic behavior and had anomalous large net magnetization. The spontaneous magnetization reached the maximum when the precursor was heat-treated at 350°C. Moreover the particles exhibited the exchange bias properties with increasing the grain size of $LaFeO_3$. The low blocking temperature observed by both magnetization and Mössbauer measurements indicated that the obtained nanoparticles at 350°C were magnetically isolated with each other.

Author details

Tatsuo Fujii[*], Ikko Matsusue and Jun Takada
Department of Applied Chemistry, Okayama University, Japan

[*] Corresponding Author

Acknowledgement

5. References

[1] Ming Q, Nersesyan MD, Wagner A, Ritchie J, Richardson JT, Luss D, Jacobson AJ, Yang YL (1999) Combustion synthesis and characterization of Sr and Ga doped LaFeO₃. Solid State Ionics 122: 113-121.

[2] Yoon JW, Grilli ML, Di Bartolomeo E , Polini R, Traversa E (2001) The NO₂ response of solid electrolyte sensors made using nano-sized LaFeO₃ electrodes. Sens Actuators B 76: 483-488.

[3] Hole I, Tybell T, Grepstad JK, Wærnhus I, Grande T, Wiik K (2003) High temperature transport kinetics in heteroepitaxial LaFeO3 thin films. Solid-State Electronics 47: 2279-2282.

[4] Toan NN, Saukko S, Lantto V (2003) Gas sensing with semiconducting perovskite oxide LaFeO₃. Physica B 327: 279–282.

[5] Parida KM, Reddy KH, Martha S, Das DP, Biswal N (2010) Fabrication of nanocrystalline LaFeO₃: An efficient solegel auto-combustion assisted visible light responsive photocatalyst for water decomposition. Int J Hyd Energy 35: 12161-12168.

[6] Su H, Jing L, Shi K, Yao C, Fu H (2010) Synthesis of large surface area LaFeO₃ nanoparticles by SBA-16 template method as high active visible photocatalysts. J Nanopart Res 12: 967-974.

[7] Szymczak R (1977) Temperature dependence of bubble domain structure in YFeO₃ and DyFeO₃ orthoferrites. Physica B+C 86-88: 1351-1353.

[8] Treves D (1965) Studies on Orthoferrites at the Weizmann Institute of Science. J Appl Phys 36: 1033-1039.

[9] Kodama RH, Berkowitz AE (1999) Atomic-scale magnetic modeling of oxide nanoparticles. Phys Rev B 59: 6321-6336.

[10] Lee YC, Parkhomov AB, Krishnan KM (2010) Size-driven magnetic transitions in monodisperse MnO nanocrystals. J Appl Phys 107: 09E124-1-3.

[11] Nakayama S (2001) LaFeO3 perovskite-type oxide prepared by oxide-mixing, co-precipitation and complex synthesis methods. J Mater Sci 36: 5643-5648.

[12] Li X, Zhang H, Zhao M (1994) Preparation of nanocrystalline LaFeO₃ using reverse drop coprecipitation with polyvinyl alcohol as protecting agent. Mater Chem Phys 37: 132-135.

[13] Popa M, Frantti J, Kakihana M (2002) Lanthanum ferrite LaFeO₃₊d nanopowders obtained by the polymerizable complex method. Solid State Ionics 154-155: 437-445.

[14] Wang JB, Liu QF, Xue DS, Li FS (2002) Synthesis and characterization of LaFeO₃ nano particles. J Matter Sci Lett 21: 1059-1062.

[15] Rajendran M, Bhattacharya AK (2006) Nanocrystalline orthoferrite powders: Synthesis and magnetic properties. J Eur Ceramic Soc 26: 3675-3679.

[16] Fujii T, Matsusue I, Nakatsuka D, Nakanishi M, Takada J (2011) Synthesis and anomalous magnetic properties of LaFeO$_3$ nanoparticles by hot soap method. Mater Chem Phys 129: 805-809.

[17] Fujii T, Matsusue I, Nakanishi M, Takada J (2012) Formation and superparamagnetic behaviors of LaFeO$_3$ nanoparticles. Hyperfine Interact 205: 97-100.

[18] Murray CB, Noms DJ, and Bawendi MG (1993) Synthesis and Characterization of Nearly Monodisperse CdE (E = S, Se, Te) Semiconductor Nanocrystallites. J Am Chem Soc 115: 8706-8715.

[19] Sun S, Murray CB, Weller D, Folks L, Moser A (2000) Monodisperse FePt Nanoparticles and Ferromagnetic FePt Nanocrystal Superlattices. Science 287: 1989-1992.

[20] Shouheng Sun S, Zeng H, Robinson DB, Raoux S, Rice PM, Wang SX, and Li G (2004) Monodisperse MFe$_2$O$_4$ (M= Fe, Co, Mn) Nanoparticles. J Am Chem Soc 126: 273-279.

[21] Sadaoka Y, Aono H, Traversa E, Sakamoto M (1998) Thermal evolution of nanosized LaFeO$_3$ powders from a heteronuclear complex, La[Fe(CN)$_6$]·nH$_2$O. J Alloys Comp 278: 135-141.

[22] Tayyari SF, Bakhshi T, Ebrahimi M, Sammelson RE (2009) Structure and vibrational assignment of beryllium acetylacetonate. Spectrochim Acta A 73: 342-347.

[23] Nakamoto K, McCarthy PJ, Martell AE (1961) Infrared Spectra of Metal Chelate Compounds. III. Infrared Spectra of Acetylacetonates of Divalent Metals. J. Am. Chem. Soc. 83: 1272-1276

[24] Gosavi PV, Biniwale RB (2010) Pure phase LaFeO$_3$ perovskite with improved surface area synthesized using different routes and its characterization. Mater Chem Phys 119: 324-329.

[25] El-Hendawy AA (2006) Variation in the FTIR spectra of a biomass under impregnation, carbonization and oxidation conditions. J Anal Appl Pyrolysis 75: 159–166.

[26] Li X, Cui X, Liu X, Jin M, Xiao L, Zhao M (1991) Mössbauer spectroscopic study on nanocrystalline LaFeO$_3$ materials. Hyperfine Interact 69: 851-854.

[27] Shen H, Cheng G, Wu A, Xu J, Zhao J (2009) Combustion synthesis and characterization of nano-crystalline LaFeO$_3$ powder. Phys Status Solidi A 206: 1420-1424.

[28] Bedanta S, Kleemaann W (2009) Supermagnetism. J Phys D Appl Phys 42: 013001-1-27.

[29] Mørup S, Frandsen S, Bødker F, Klausen SN, Lefmann K, LindgÅrd PA, Hansen MF (2002) Magnetic Properties of Nanoparticles of Antiferromagnetic Materials. Hyperfine Interact 144/145: 347-357.

[30] Bødker F, Hansen MF, Koch CB, Lefmann K, Mørup S (2000) Magnetic properties of hematite nanoparticles. Phys Rev B 61: 6826-3838.

[31] Ahmadvand H, Salamati H, Kameli P, Poddar A, Acet M, Zakeri K (2010) Exchange bias in LaFeO$_3$ nanoparticles. J Phys D Appl Phys 43: 245002-1-5.